Research Square

Preprints are preliminary reports that have not undergone peer review.
They should not be considered conclusive, used to inform clinical practice,
or referenced by the media as validated information.

Deus ex machina long-term cooling of the eastern Pacific cold tongue in ocean reanalysis data

Feng Jiang

fjiang@ldeo.columbia.edu

Lamont Doherty Earth Observatory of Columbia University

Richard Seager

Lamont Doherty Earth Observatory of Columbia University

Mark A. Cane

Lamont Doherty Earth Observatory of Columbia University

Research Article

Keywords:

Posted Date: January 14th, 2026

DOI: https://doi.org/10.21203/rs.3.rs-8586447/v1

License: This work is licensed under a Creative Commons Attribution 4.0 International License.
Read Full License

Additional Declarations: The authors declare no competing interests.

Deus ex machina long-term cooling of the eastern Pacific cold tongue in ocean reanalysis data

Feng Jiang,[a] * Richard Seager,[a] Mark A. Cane.[a]

[a] *Lamont-Doherty Earth Observatory, Columbia University, Palisades, NY, USA*

**Corresponding Author:* Feng Jiang, fjiang@ldeo.columbia.edu

ABSTRACT

The emergence of an observed distinctive, meridionally confined surface cooling trend in the tropical Pacific cold tongue over recent decades contrasts sharply with the rapid warming simulated by most climate models, representing a key unresolved feature of climate change. Ocean-only simulations, even when forced with observed atmospheric conditions, likewise fail to reproduce the observed long-term absence of surface layer warming over the eastern Pacific cold tongue. Here we examine the long-term heat budget of the surface layer in the equatorial Pacific using atmospheric and oceanic reanalysis data, quantifying contributions from surface heat fluxes, ocean advection, and vertical diffusion inferred through Richardson number-based diffusivity estimates. In the Ocean ReAnalysis System 5 (ORAS5), the observed cold tongue cooling cannot be reproduced by the model's intrinsic dynamics alone; instead, it depends on a surface heat flux adjustment imposed during data assimilation. A reduction in the warming effect associated with this adjustment in the eastern Pacific cold tongue over time emerges as the dominant contributor to the long-term cooling in the reanalysis data, a *deus ex machina* obscuring the actual physical drivers of change in the real ocean. We discuss potential origins of this *deus ex machina* cooling effect, including the influence of analysis increments, uncertainties in surface forcing and possible problems in the representation of oceanic processes, particularly subsurface turbulent heat flux induced by oceanic mixing processes. This work emphasizes that reanalysis-based assessments remain subject to inherent biases from the ocean models they are built upon. Resolving the discrepancy between observed and simulated Pacific trends will require confronting the structural limitations of models.

1. Introduction

A critical aspect of the long-term sea surface temperature (SST) trend in the Pacific cold tongue region is the actual SST cooling observed across the central-to-eastern equatorial Pacific during recent decades, despite continued warming in the western Pacific warm pool (Lee et al. 2022; Seager et al. 2022). In contrast, the vast majority of models under historical radiative forcings simulate the opposite with faster warming in the eastern Pacific than in the west (Watanabe et al. 2021; Wills et al. 2022; Byrne et al. 2025). Resolving this discrepancy between observations and model simulations is critical for understanding the tropical Pacific's response to anthropogenic forcing and for projecting regional climate change worldwide (Sobel et al. 2023; Seager et al. 2023; Watanabe et al. 2024) and, potentially, transient and equilibrium climate sensitivity (Rose et al. 2014; Gregory and Andrews 2016; Andrews et al. 2022; Rugenstein et al. 2023; Armour et al. 2024). Growing consensus points to systematic model biases as the main source of the mismatch (Seager et al. 2019; Kim et al. 2022; Wills et al. 2022; Simpson et al. 2025; Zhuo et al. 2025), yet debate continues over whether the apparent agreement of some models with observations reflects improved physics or coincidental internal variability (Dong and Zhou 2014; Meehl et al. 2016; Coats and Karnauskas 2017; Watanabe et al. 2021; Seager et al. 2022; Yeager et al. 2023; Jiang et al. 2024a, 2025; Dhame et al. 2025). Regardless, even these climate model simulations fail to approximate the recent long-term (e.g. 1950s to now) SST trend pattern in the real world of a meridionally confined strip of cooling in the eastern equatorial Pacific (Seager et al. 2022; Jiang et al. 2024a), which we label the Pacific Climate Change (PCC) pattern (Jiang et al. 2024a).

Quantitative analysis of the processes driving the observed PCC pattern is challenging because of the difficulty of closing the heat budget and accurately quantifying atmospheric and oceanic processes using long-term observational or reanalysis datasets. In our previous work (Jiang et al. 2024a,b), we conducted heat budget analyses for the upper Pacific Ocean using ocean reanalysis data to understand historical changes. A key finding there, and critical to the PCC pattern, was identification in observations and ocean reanalyses of a long-term cooling of subsurface waters and shoaling of the thermocline that is driven by Ekman pumping in the central-to-eastern Pacific west of ~140°W and reduced shear-driven mixing in the east. In the presence of upwelling and vertical mixing the subsurface cooling is here hypothesized to be key to explaining the cold tongue cooling. However, two key components of the upper ocean heat budget and its relation to SST – surface heat flux and oceanic mixing processes – remain poorly quantified in the context of the PCC pattern.

Reliable quantification of air-sea fluxes is notoriously difficult, largely due to uncertainties in measuring flux-related variables and in parameterizing boundary layer processes (Isemer et al. 1989; Josey et al. 1999; Large et al. 1997; Brunke et al. 2003; Berry and Kent 2009; Large and Yeager 2009; Dee et al. 2011; Rienecker et al. 2011; Bentamy et al. 2017; Liu et al. 2017; Tang et al. 2024). Moreover, the climate change signal is inherently difficult to isolate in the presence of strong internal variability, and the accuracy required often exceeds the capabilities of current observational systems (Gulev et al. 2007; Yu 2019). Significant discrepancies exist in estimates of long-term trends in globally averaged surface heat flux across datasets and, at regional scales even the sign of the change can differ among them (Rahul and Gnanaseelan 2013; Tang et al. 2024). Ocean reanalysis products also provide net surface heat fluxes (Valdivieso et al. 2017). However, in many ocean reanalysis products, surface heat fluxes are computed interactively from near-surface atmospheric state variables and the model-simulated SST at each time step via the CORE bulk formula (Large and Yeager 2009). These fluxes are subsequently adjusted so SST closely matches observations through data assimilation and surface flux nudging. For instance, in the Ocean ReAnalysis System 5 (ORAS5) data, the non-solar component of the total surface heat flux in the SST equation is adjusted to compensate for model biases and deficiencies, particularly in surface layer temperature (Zuo et al. 2019). The reported net surface heat flux includes these adjustments.

Compounding these challenges is the difficulty of quantifying turbulent oceanic mixing and its long-term variability. In the upper equatorial Pacific Ocean, wind-driven and shear-related subsurface turbulent heat flux induced by oceanic mixing processes acts to homogenize the temperature vertically by diffusively redistributing heat gained at the surface downward and entraining colder subsurface water into the mixed layer (Liu et al. 2005; Ray et al. 2018a,b; Yang et al. 2014). Vertical mixing plays a crucial role in the formation and persistence of the cold tongue (Deppenmeier et al. 2022; Holmes et al. 2019), as well as in modulating variability across different timescales (Moum et al. 2009, 2013; Pham et al. 2017; Warner and Moum 2019; Nakamura et al. 2024; Liu et al. 2025; Tozuka 2025). However, there are few measurements of vertical mixing across hourly, daily and monthly timescales since the 1950s, hindering a full understanding of the dynamics underlying the historical cold tongue cooling.

In this study, we examine the heat budget of the Pacific cold tongue on climate change timescales using oceanic and atmospheric reanalysis data. Our goal is to discover what physical processes caused the cold tongue cooling; however, our results show that the ocean reanalysis does not generate the cooling on its own. It must be imposed by an adjustment to the surface heat flux inconsistent with atmospheric reanalysis estimates. This adjustment-driven cooling is

a "*deus ex machina*" that obscures the physical processes actually responsible for cold tongue temperature change. We then discuss several possible reasons for this adjustment-driven cooling, including the influence of analysis increments, uncertainties in surface forcing as well as problems in the representation of oceanic processes.

2. Data and methodology

We first examine the observed long-term SST trend in the tropical Pacific and compare it with trends simulated by the Coupled Model Intercomparison Project Phase 6 (CMIP6) models. We then evaluate surface layer temperature changes in ocean reanalysis products and contrast them with Ocean Model Intercomparison Project Phase 2 (OMIP2) simulations. To diagnose the processes driving the observed SST trends, we further analyze the surface layer heat budget using ocean and atmospheric reanalysis data. The observational and reanalysis datasets, model simulations, and methods used in this study are described below.

The observed monthly SST and sea ice analysis is obtained from the Met Office Hadley Centre (HadISST) at a horizontal resolution of 1°×1° (Rayner et al. 2003) during 1958–2024. The monthly surface heat fluxes including latent heat flux, sensible heat flux, shortwave and longwave radiation are obtained from the European Center for Medium-Range Weather Forecasts (ECMWF) Reanalysis v5 (ERA5) with a horizontal resolution of 0.25°×0.25° (Hersbach et al. 2020). We also examine oceanic variables including monthly subsurface temperature, zonal and meridional current data and surface net heat flux data from ORAS5, the latest ocean reanalysis product provided by European Centre for Medium-Range Weather Forecasts (ECMWF) during 1958–2024 (Zuo et al. 2019). Vertical velocity in the ocean is computed from ORAS5 horizontal currents using mass continuity by an upward integration of the horizontal divergence from the bottom (Vidard et al. 2015). As our calculation does not consider realistic boundary conditions at the surface and bottom and is not conducted on the native model grid, a degree of error is likely introduced. ORAS5 has a horizontal resolution of 0.25° and 75 vertical levels with a finer 1-m resolution near the surface and uses the Nucleus for European Modeling of the Ocean (NEMO) model driven by atmospheric surface forcing from ECMWF, and constrained by in situ assimilation, SST nudging and bias correction (Balmaseda et al. 2015; Zuo et al. 2017, 2019). ORAS5 is forced by different generations of ECMWF atmospheric reanalysis products as boundary conditions: ERA-40 prior to 1979, ERA-Interim from 1979 to 2014, and ECMWF NWP from 2015 onward (Zuo et al. 2019). Monthly surface heat flux components from the Japanese 55-year Reanalysis (JRA-55) provided by the Japan Meteorological Agency (JMA) during 1958–2018 are also utilized for

comparison. In addition, daily subsurface temperature and horizontal current data from the Global Ocean Reanalysis and Simulations (GLORYS) (Lellouche et al. 2021) version 12V1 during 1993–2024 are used in the Appendix to validate calculations based on monthly ORAS5 outputs.

To assess model–observation discrepancies, we also analyze SST from the 32 CMIP6 models (historical simulations during 1958–2014 extended with SSP3-7.0 to 2024) in Supplementary Table 1 (Eyring et al. 2016; O'Neill et al. 2016). We also analyze subsurface temperature data from 15 models participating in OMIP2 (Supplementary Table 2) during 1958–2018 to compare with ORAS5. OMIP was designed to evaluate and identify systematic biases in coupled models, particularly those originating from the ocean-sea ice component (Griffies et al. 2016). In OMIP2, the ocean models are forced by the JRA55-do dataset from 1958 to 2018 including surface wind, air temperature, humidity, longwave and shortwave radiation, and precipitation fluxes (Tsujino et al. 2018, 2020), which is a modified version of JRA-55 (Kobayashi et al. 2015). We also analyze surface heat flux including latent heat flux, sensible heat flux, shortwave radiation, and longwave radiation from 5 out of the 15 models, where data were available.

All variables are interpolated to a horizontal resolution of 1° × 1°. For consistency, all radiative and surface heat flux components (in units of W/m^2) are converted to their equivalent contributions to SST (in units of °C/month) by dividing by $C_p\rho_0 d$, where C_p is the specific heat capacity of seawater (4184 J/kg/°C), ρ_0 is the reference ocean density (1024 kg/m^3), and d is 50 m. By convention, positive values indicate a net heat gain by the ocean, and negative values indicate a net heat loss to the atmosphere.

We establish the vertically integrated heat budget of the surface layer in ORAS5, which is given by:

$$\frac{1}{d}\int_{-d}^{0}\left(\frac{\partial T}{\partial t}\right)dz = \frac{1}{d}\int_{-d}^{0}(Q_{adv})dz + Q_{net} - Q_{pen} + Q_{res}, \qquad \text{Eq. (1)}$$

where Q_{net} is the net heat flux provided by ORAS5 defined positive downward. Q_{pen} is the portion of shortwave radiation (Q_{short}) that penetrates below the layer, which taken as $Q_{pen} = \frac{Q_{short}}{C_p\rho_0 d} * (0.58e^{\frac{-d}{0.35}} + 0.42e^{\frac{-d}{23}})$ as in ORAS5. A constant value of 50 m is used for the layer depth d so the surface layer here is not identical to the ocean mixed layer. For d = 50 m, Q_{pen} is around 5% of Q_{short}. Since ORAS5 does not provide individual surface flux components, and solar radiation should be nearly identical between ERA5 and ORAS5, we use Q_{short} from

ERA5 to calculate Q_{pen} in Eq. (1). Q_{adv} represents the dynamical advection terms, expressed as $Q_{adv} = -u\frac{\partial T}{\partial x} - v\frac{\partial T}{\partial y} - w\frac{\partial T}{\partial z}$. Q_{res} is the residual in (1) needed to make the equation balance. It includes turbulent mixing, subgrid/submonthly variabilities, influences from data assimilation and computing errors but will also be influenced by a surface heat flux adjustment as we will discuss below.

3. Contrasting long-term SST and surface layer temperature trends in observations/reanalysis and model simulations

Observations show a narrow band of SST cooling over the equatorial central-to-eastern Pacific and along the southern equatorial coast of South America (Fig. 1a). Over the same period, CMIP6 models simulate overall warming across the equatorial Pacific, with a maximum in the far eastern equatorial Pacific (Fig. 1b). The discrepancy is evident in Figure 1c, where observations show pronounced equatorial warming in the western Pacific warm pool, weak warming to slight cooling in the central-to-eastern Pacific, and enhanced warming near the South American coast. In contrast, the CMIP6 multi-model mean (MMM) shows nearly uniform warming across the equatorial Pacific, with a maximum east of 120°W. This mismatch has been linked to systematic biases in climate models, including the excessive cold tongue (Fig. 1d) as well as biases in surface fields, including overly weak winds and unrealistically high relative humidity (Luo et al. 2018; Seager et al. 2019; Wills et al. 2022; Simpson et al. 2025).

Even in OMIP2 simulations forced with observed atmospheric conditions, the discrepancy in upper ocean temperature trends persists over the equatorial Pacific cold tongue. In ORAS5, the surface layer temperature trend (Fig. 2a) closely resembles the SST trend (Fig. 1a), showing a slight cooling in the eastern equatorial Pacific. In contrast, all ocean-only experiments exhibit a pronounced warming trend in the same region (Fig. 2b and c), despite the prescribed observational forcing. Note that among the 15 OMIP2 models, three are based on NEMO (CMCC-CM2, CNRM-CM-6-1 and EC-Earth3), which is also the ocean model underlying ORAS5, and their representation of surface layer temperature trends does not differ markedly from the other models (Fig. 2c). This discrepancy is surprising, but it should be remembered that ocean models retain inherent mean state biases even under prescribed atmospheric forcing. For example, the climatological surface layer temperature in OMIP2 simulations relative to ORAS5 during 1958–1977 shows a warm bias in the western Pacific and a cold bias in the east, reaching up to ~1°C (Fig. 2d). The bias pattern in surface layer temperature differs from that

in SST along the South American coast, where the warm bias is confined to a very shallow near-surface layer, and cold bias dominates at depth (not shown but see Wittenberg et al. 2018; Reichl et al. 2024).

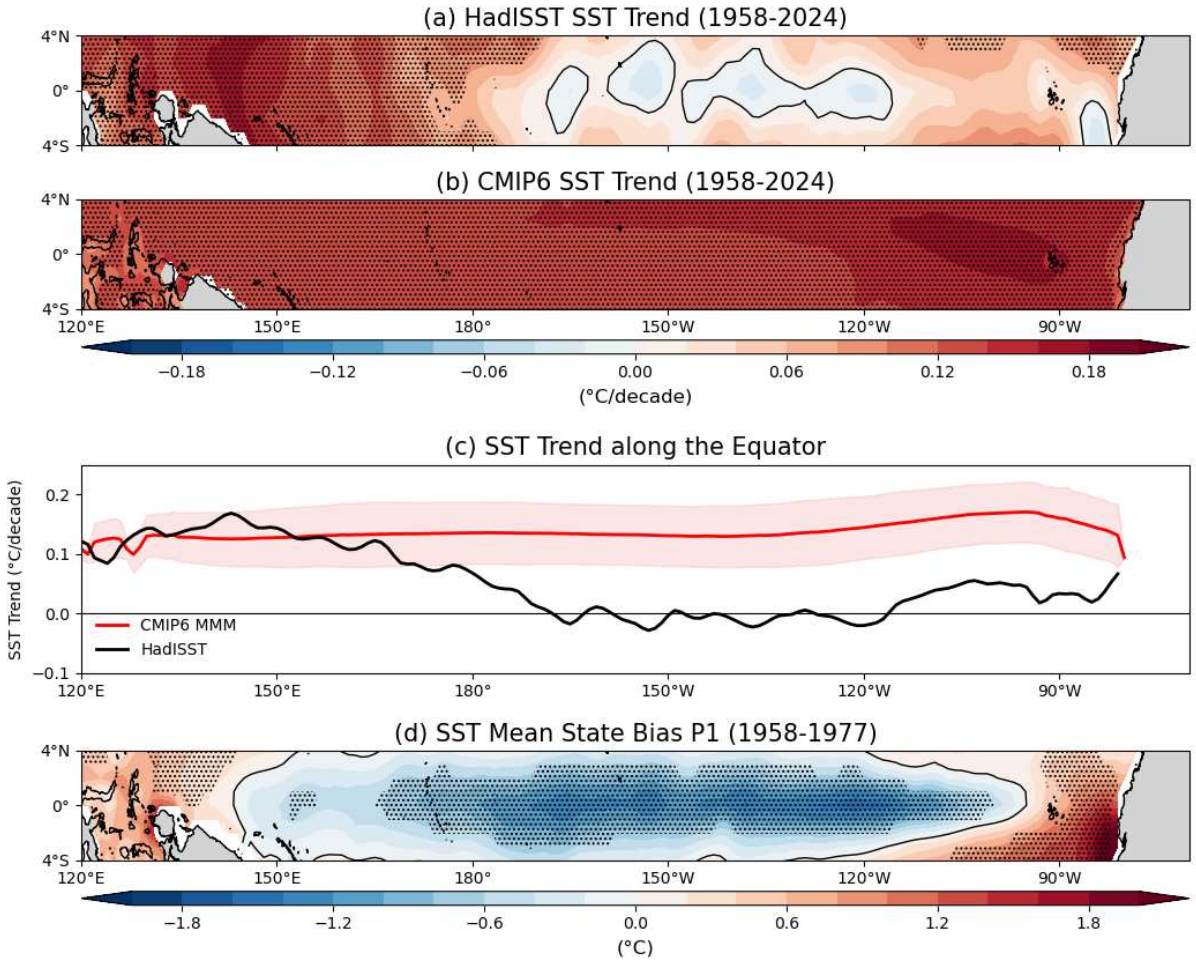

Figure 1. (a) SST trend during 1958–2024 (°C/decade) based on HadISST. (b) CMIP6 MMM SST trend during 1958–2024 (°C/decade), using historical simulations for 1958–2014 extended to 2024 with SSP3-7.0. (c) Equatorial (1°S–1°N averaged) distribution of SST trends in HadISST and the CMIP6 MMM. (d) CMIP6 MMM SST mean state bias during 1958–1977 relative to HadISST. Stippling in (a) marks regions where the trend is significant at the 95% level based on the two-tailed Student's *t* test with n−2 degrees of freedom, where n is the sample size. In (b) and (d), stippling marks regions where at least 75% of models agree on the sign of the trend (b) or on the sign of the bias (d).

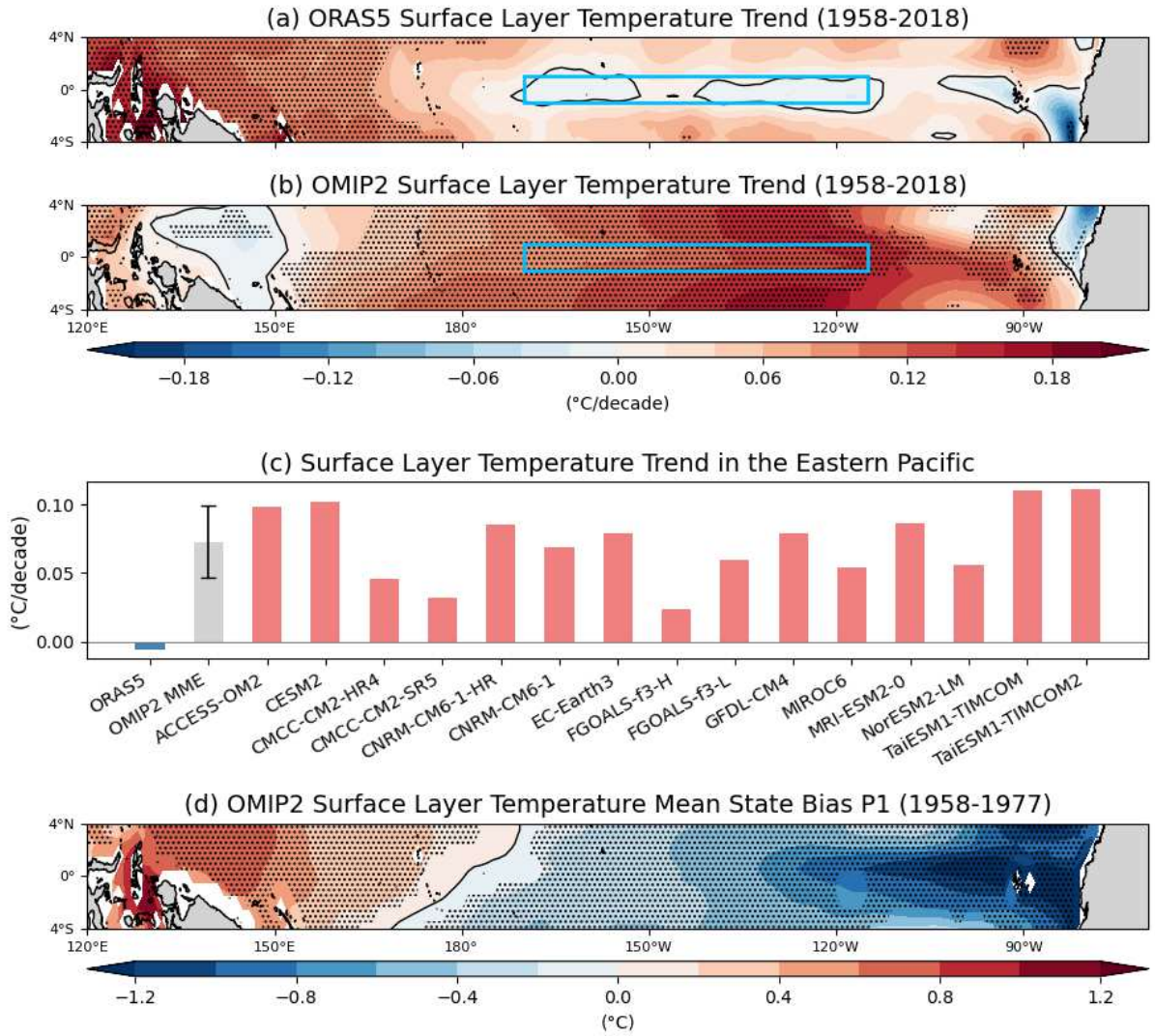

Figure 2. Surface layer (50 m averaged) temperature trend during 1958–2018 (°C/decade) based on **(a)** ORAS5 and (b) OMIP2 MMM. (c) Surface layer temperature trend (°C/decade) over the eastern equatorial Pacific (blue box in (a-b), 1°S–1°N, 190°E–245°E) during 1958–2018 based on ORAS5, the OMIP2 MME, and individual OMIP2 models. (d) OMIP2 MMM bias in the surface layer temperature (°C) relative to ORAS5 during 1958–1977. Error bars in (c) represent ±0.5 standard deviations across the OMIP2 ensemble. In (a), stippling marks regions where the trend is significant at the 95% level based on the two-tailed Student's *t* test. In (b) and (d), stippling marks regions where at least 75% of models agree on the sign of the trend (b) or on the sign of the bias (d).

4. Surface layer heat budget estimates in reanalysis data on climate change timescales.

To understand the dynamics underlying the SST trend over the equatorial Pacific cold tongue in ORAS5, we analyze the heat budget of the surface layer (upper 50 m), as its trend pattern reasonably matches that of HadISST (Figs. 1a and 2a). Applying the heat budget equation (Eq. (1)) to interpret long-term trends in surface layer temperature over the equatorial Pacific is difficult. The SST trend in the equatorial Pacific is typically on the order of one

degree over several decades (i.e. ~10^{-3} °C/month), while temperature variability associated with the El Niño–Southern Oscillation on interannual timescales is one degree over a few months, making it challenging to isolate a robust climate change signal in the eastern equatorial Pacific (Solomon and Newman 2012; Lee et al. 2022).

To understand the dynamics underlying the climate change, we follow an approach (Jiang et al. 2024a,b) in which we compare heat budget terms between two time periods: the reference period P1 when the climate change signal is weak and a more recent period P2 when the signal is more prominent. Here we define P1 as 1958–1977 and P2 as 2005–2024. Our results are not sensitive to the small shifts in these windows, provided that the reference lies within the early decades of the record (e.g., 1959–1978) and the climate change period includes recent years (e.g., 2004–2023). Averaged over the reference period P1, the heat budget is a balance among large terms. The climatological warming due to Q_{net} (Fig. 3a) and the cooling rate due to Q_{adv} (Fig. 3b) are both on the order of 1°C/month at the equator. The long-term temperature trend in the equatorial Pacific is only ~ 0.1% of the Q_{net} and Q_{adv} terms. Thus, while the climate is undergoing a transient adjustment toward a new equilibrium state due to radiative forcing, the ocean system is well approximated as being in a quasi-equilibrium state, with a very small temperature tendency term that is a small residual from the near-exact cancellation of much larger terms (right-hand-side of Eq. (1)). Since this residual is orders of magnitude smaller than the individual terms, even modest uncertainties in those terms can be comparable to or larger than the residual itself, rendering it highly sensitive to observational and computational uncertainties (Yu 2019).

As shown in Figure 3b, the net effect of advection is to cool the surface layer, primarily via vertical advection by upwelling colder subsurface water to the surface, which is then advected poleward and westward. However, this dynamical cooling only partially compensates for the warming effect of $Q_{net} - Q_{pen}$ at the equator, leaving a large residual cooling term (Fig. 3c). This large residual is expected given that the ORAS5 does not archive mixing terms. In the central-to-eastern equatorial Pacific, the residual includes the vertical mixing that redistributes heat downward through shear-driven mixing, cooling the surface layer and playing an important role in maintaining the cold tongue (Deppenmeier et al. 2022; Holmes et al. 2019; Ray et al. 2018a).

Comparing P2 to P1, the net surface heat flux term Q_{net} based on ORAS5 shows a robust cooling effect in the equatorial Pacific (Fig. 3d), while the net advective effect leads to scattered warming near the equator in the central-to-eastern Pacific and contributes to surface layer

cooling north and south of the equator (Fig. 3e). As shown in our previous work (Jiang et al. 2024b), the net advective warming tendency in the equatorial region is primarily the difference of warming due to zonal advection and cooling due to vertical advection, with a minor contribution from meridional advection.

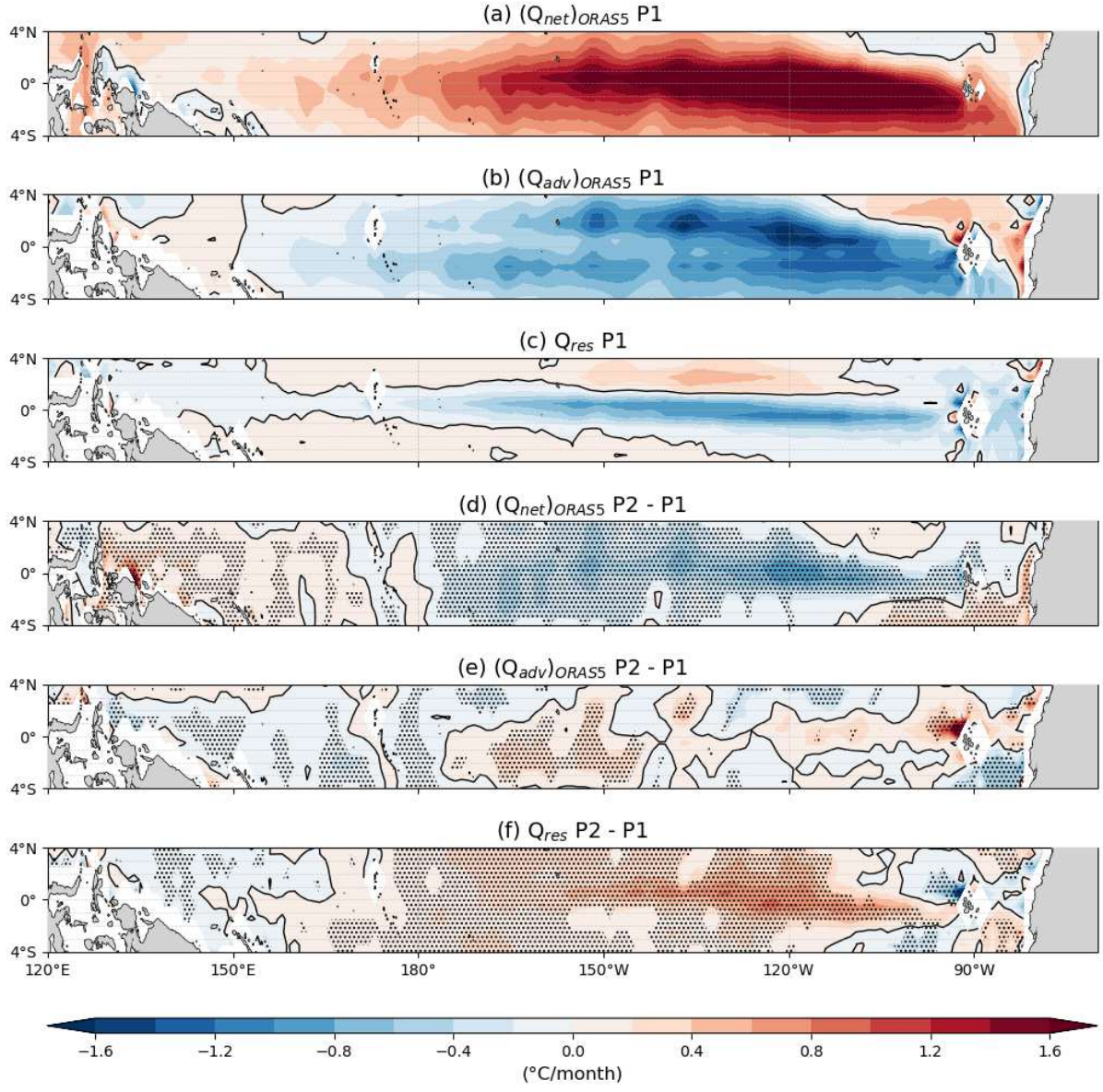

Figure 3. (a) Climatological net surface heat flux Q_{net} (°C/ month) in P1 (1958–1977) based on ORAS5. (b) Climatological surface layer averaged dynamical advection Q_{adv} based on ORAS5 (°C/ month). (c) Residual term Q_{res} (°C/ month) in P1 based on Eq. (1). (d) Difference in net surface heat flux Q_{net} (°C/month) between P2 (2005–2024) and P1 (1958–1977) based on ORAS5. (e) Difference in surface layer averaged advection term Q_{adv} (°C/month) between P2 and P1 based on ORAS5. (f) Difference in residual term Q_{res} (°C/month) between P2 and P1 based on ORAS5. Stippling in (e-f) marks regions where the difference between P2 and P1 is significant at the 95% level based on the two-tailed Student's *t* test.

Fig. 3f shows that the change in the residual term Q_{res} between P2 and P1 contributes substantially to surface layer warming. Since mixing terms are not archived in ORAS5, they are included in Q_{res} . We estimate the vertical diffusive flux using a Richardson number (Ri)-dependent parameterization scheme described in the Appendix. As shown in Figure A1, the climatological vertical diffusion in P1 using the monthly temperature gradient and eddy diffusivity inferred from monthly Richardson numbers Q_{diffu} (Fig. A1) captures the large-scale sign and zonal structure of the residual cooling in Figure 3c over the central-to-eastern equatorial Pacific (180°–90°W), but there are substantial differences in magnitude. We similarly calculate the Ri-based eddy diffusivity in P2 and estimate the corresponding diffusion term (Fig. A1b). As shown in Figure A1c, the change in the Ri-based diffusion term Q_{diffu} results in surface layer warming along the equator that is quantitatively consistent with the change in the residual at the equator (Fig. 3f). It is well-known that vertical mixing is exceptionally strong at the equator, and this calculation suggests that it is the greatest part of the residual needed to close the heat budget. A more definitive statement would be possible if the actual ORAS5 mixing term had been saved.

5. *Deus ex machina* cooling in reanalysis data

Based on analysis of ORAS5, Q_{net} is the only robust cooling term in the equatorial Pacific from P1 to P2. As noted in Section 1, ORAS5 Q_{net} is not the real-world air–sea flux. Ocean reanalysis data is inherently dependent on ocean models. When included in climate models, across multiple generations ocean models have had persistent systematic biases that contribute to an excessively cold and overly westward-extended cold tongue, as well as warm SST biases near the South American coast (Li and Xie 2014; Figures 1d and 2d). These systematic mean state biases are not only present in free-running long-term simulations or those driven by historical external forcings, but also tend to develop quickly within months after initialization in seasonal forecast models, including those from ECMWF (Pillai et al. 2021; L'Heureux et al. 2022). To compensate for such biases and reproduce observed surface temperature distributions, ocean reanalysis data like ORAS5 apply additional heat flux "adjustments" (Valdivieso et al. 2017). As Browne et al. (2019) and Zuo et al. (2019, from which this quotation is taken) describe: "SST is assimilated in ORAS5 by modifying the surface non-solar total heat flux using the product of a globally uniform restoration term of 200 W m^{-2} K^{-1} and the difference between modelled and observed SST". This non-solar surface heat flux adjustment plays a central role in reducing tropical Pacific surface temperature biases

(Zuo et al. 2019; their Figs. 17–18). We treat the net surface heat flux from ERA5 as the "true" surface flux, since it was computed from the observed SST, the same SST used in the ORAS5 data assimilation (Hersbach et al. 2020). The adjusted net surface heat flux in ORAS5 can then be expressed as:

$$(Q_{net})_{ORAS5} = (Q_{net})_{ERA5} + Q_{adjust} \quad \text{Eq. (2)}$$

where $(\,)_{ORAS5}$ and $(\,)_{ERA5}$ denote the terms reported in ORAS5 and ERA5 data, respectively, and Q_{adjust} indicates the flux adjustment required for the NEMO model underlying ORAS5 to reproduce the observed SST. At the surface, this adjustment is applied over short damping timescales to nudge the model toward observed SSTs, using a restoration term of 200 $W/(m^2 * ℃)$ and the difference between modelled and observed SST (Balmaseda et al. 2013; Zuo et al. 2019). Thus, even a modest temperature discrepancy of 0.25 ℃ implies a continuous adjustment heat flux of 50 W/m^2, which would adjust the temperature of a 50 m mixed layer by that amount over an e-folding timescale of ~10 days.

According to ERA5, the SST cooling in P2 compared to P1 in the equatorial eastern Pacific is accompanied by an increase in local net (downward) surface heat flux, while regions to the north and southeast that experience surface warming show a decrease in net heat flux (Fig. 4a). The net surface heat flux change between P2 and P1 along the equator is primarily driven by changes in latent heat flux (Fig. 4b). A similar pattern in latent heat flux change is also evident in a previous long-term trend estimate based on the Objectively Analyzed Air-Sea Fluxes (OAFlux) dataset originating from ship observations, atmospheric reanalysis and remote-sensed data for the period 1958–2013 (Yang et al. 2016). In most parts of the tropical ocean, SST warming and intensified surface winds have led to enhanced evaporation and latent heat loss (Liu and Curry 2006; Yu and Weller 2007; Li et al. 2011; Yang et al. 2016). In contrast, in the equatorial Pacific between 150°W and 120°W the SST has not warmed, wind speeds have weakened and the latent heat flux has decreased (Li et al. 2011; Yang et al. 2016), increasing the net heat flux into the ocean (Fig. 4a and b). This change is a strengthening of the climatological arrangement in which ocean processes generate the cold tongue which reduces turbulent surface heat loss and leads to a net uptake of heat from the atmosphere to the ocean.

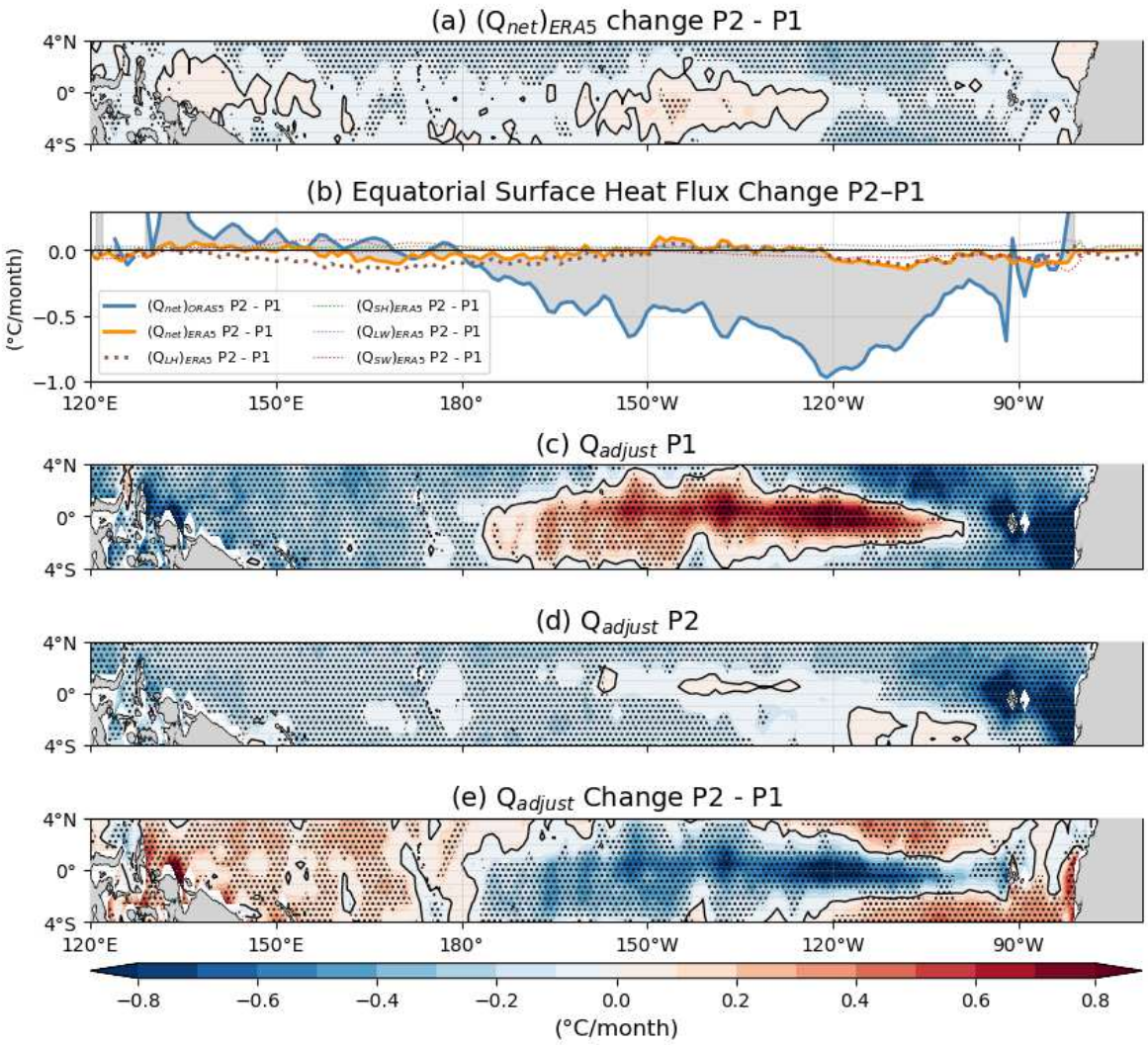

Figure 4. Difference between P2 (2005–2024) and P1 (1958–1977) based on ERA5 for (a) net surface heat flux Q_{net} (°C/month); (b) Equatorial (1°S–1°N averaged) distribution of ERA5 Q_{net} (°C/month), latent heat flux Q_{LH} (°C/month), sensible heat flux Q_{SH} (°C/month), shortwave radiation Q_{SW}, and longwave radiation Q_{LW} (°C/month). Climatological adjustment term Q_{adjust} (°C/ month) based on Eq. (2) in (c) P1 (1958–1977) and (d) in P2 (2005–2024). (e) Difference in Q_{adjust} (°C/month) between P2 and P1. Stippling in (a) and (e) marks regions where the difference between P2 and P1 is significant at the 95% level based on the two-tailed Student's *t* test. Stippling in (c) and (d) marks regions where the difference between ERA5 Q_{net} and ORAS5 is significant at the 95% level.

During P1, the adjustment term adds heat to the central-to-eastern equatorial Pacific and removes heat near the coast (Fig. 4c), reflecting a correction for the well-known excessive cold tongue SST bias pattern in the equatorial Pacific (Fig. 1d). While the adjustment term is very large in P1, during P2 the adjustment term is close to zero west of 110°W (Fig. 4d). The reduction in this adjustment term is the dominant contributor to the long-term cooling in the ocean reanalysis data (Fig. 4e). That is, a *deus ex machina* cooling surface flux adjustment must be imposed over the central-to-eastern equatorial Pacific to align the simulation with the

long-term cooling SST trend observed in HadISST. This is in marked contrast to the observed climatological arrangement where it is ocean processes that generate the cold tongue while surface heat fluxes provide an offsetting warming (Fig. 3a and b).

If the ERA5 surface fluxes are correct, at least in sign, the above analysis indicates the ocean heat movement by currents or mixing generates the cooling trend while the surface flux changes damp the SST response, which is an intensification of the climatological pattern of cooling by vertical processes offset by surface heat uptake. However, such a cooling effect does not appear in the directly computed dynamical terms or in the inferred mixing term whether based on Richardson number or the residual. We hypothesize that, instead, an additional flux adjustment term is needed to stand-in for an unrealized, due to model biases, increase in cooling by ocean processes from P1 to P2.

One possible reason that the adjustment term is larger in the first period than in the second is the increase in observational data with time. Perhaps the atmospheric data in the early period is inadequate to estimate the surface heat and momentum fluxes driving the ocean model, and oceanic observations are too few and far between for the data assimilation to replace problem areas with observed ocean data.

A second explanation for the reduced adjustment term in recent periods is that there is a compensating error within the reanalysis system that emerges when the climate change signal becomes pronounced. As is ubiquitous in coupled climate models (e.g., Seager et al. 2019; Jiang et al. 2025) (see also Fig. 1d), the ocean model underlying ORAS5 has a cold bias along the central-to-eastern equatorial Pacific (Fig. 2d), which could lead to a biased warming response to greenhouse gas forcing, with models showing excessive eastern Pacific warming compared to observations (Figs. 1a,b and 2a,b). In CMIP6, the excessive warming trend partially offsets the mean-state cold bias relative to HadISST during P2 (2005–2024) over the central-to-eastern equatorial Pacific (Fig. 5a). Similarly, over the last 20 years of OMIP2 simulations (1999–2018), the mean state bias of surface layer temperature in the central-to-eastern equatorial Pacific has largely diminished between 170°E and 110°W relative to ORAS5 (Fig. 5b). As a result, these climate model results suggest a possible error compensation mechanism is likely at play in ORAS5: the ocean model misrepresented some processes in maintaining the cold tongue climatology, introducing a cold bias in the surface layer that cannot be overcome even when the atmospheric conditions are prescribed, while simultaneously misrepresenting the response to radiative forcing, leading to an erroneous warming bias. Together, these two biases can offset one another, reducing the apparent need for additional surface heat flux adjustments in the recent period.

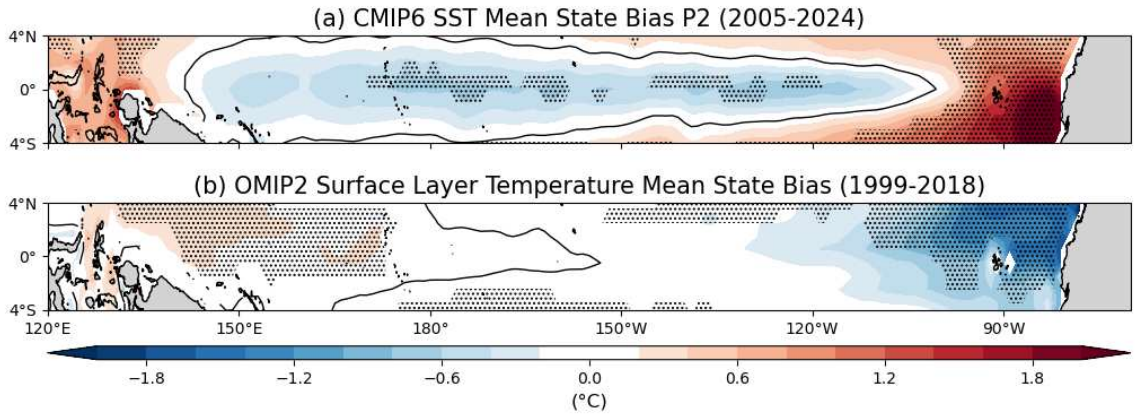

Figure 5. (a) CMIP6 MMM SST mean state bias during P2 (2005–2024) relative to HadISST. (b) OMIP2 MMM surface layer temperature mean state bias (°C) during the last 20 years of OMIP2 simulations relative to ORAS5. Stippling marks regions where at least 75% of models agree on the sign of the bias.

One caveat is that ORAS5 differs from the wind-driven OMIP2 experiments not only in that it includes data assimilation and surface heat flux adjustment, but also a different atmospheric boundary forcing dataset, which enters the bulk formula calculation. ORAS5 is forced by atmospheric fields from ECMWF, whereas OMIP2 simulations use a modified version of the JRA-55 reanalysis from JMA. In these ocean-only experiments, the surface boundary layer conditions including air temperature and humidity, which are closely coupled to the SST (Betts and Ridgway 1989; Bretherton 1993; Seager et al. 1995), that enter the bulk formula calculations of surface heat flux are prescribed (Large and Yeager 2009). These differences may also contribute to the discrepancy in the oceanic response and surface layer temperature trends in ORAS5 and OMIP2. However, as shown in Figure 6, these are unlikely to be the primary reason for the opposing long-term surface temperature trends over the eastern equatorial Pacific in ORAS5 and OMIP2. Figure 6a shows that OMIP2 simulations have increased net surface heat flux into the ocean in the western Pacific and decreased heat flux in the east. The reduction in the east is largely driven by more latent heat flux out of the ocean, which helps cool the ocean surface (Fig. 6b). However, these trend patterns are opposite in sign to those in the JRA-55, the presumed atmospheric state prescribed in the forcing for OMIP2, where the net surface heat flux decreases in the west (leading to surface cooling) and increases in the east (leading to surface warming), with the changes again dominated by latent heat flux (Fig. 6c and d). This JRA-55 heat flux trend is qualitatively consistent with ERA5 (Fig. 3e). This consistency again suggests that a biased response inherent in the ocean is responsible for the pronounced surface warming in the cold tongue region in OMIP2.

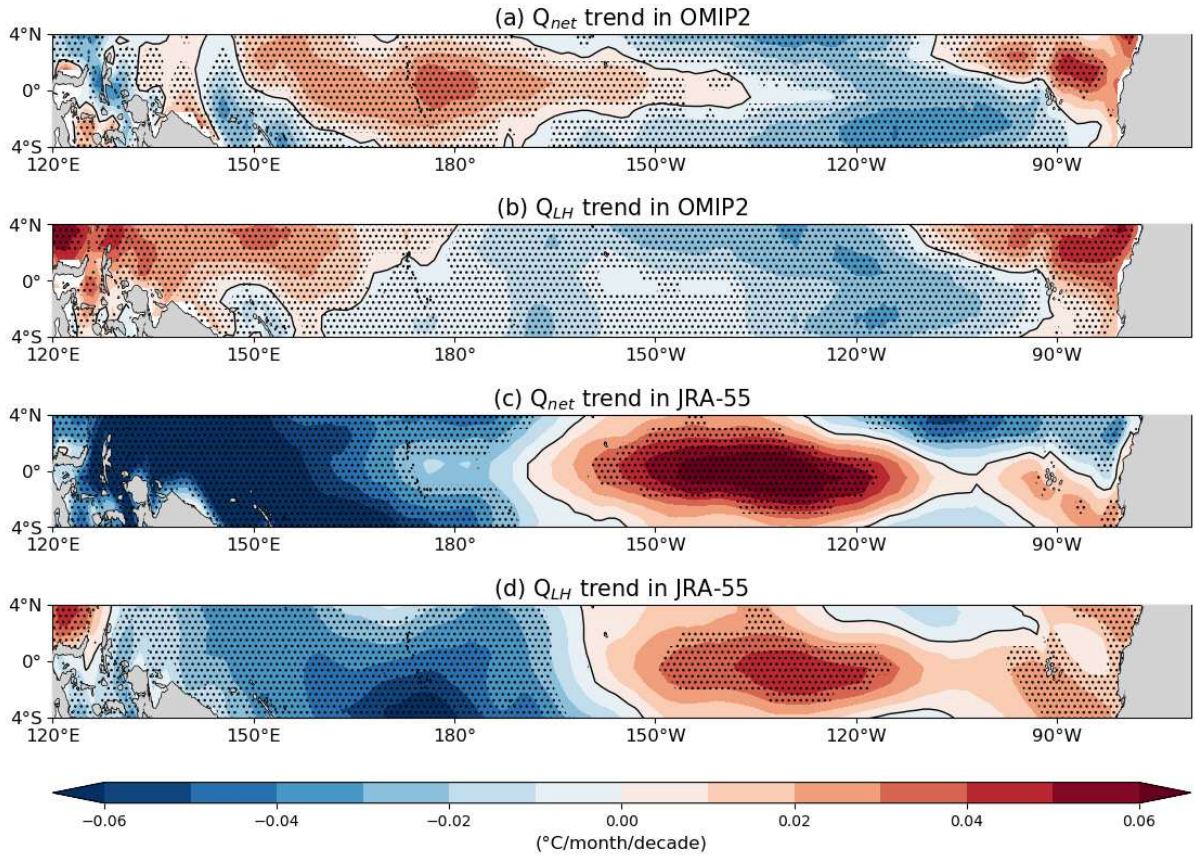

Figure 6. (a) Multi-model mean trend in net surface heat flux Q_{net} for 5 OMIP2 simulations with available data during 1958–2018 (°C/month/decade). (b) Similar to (a) but for latent heat flux Q_{LH}. (c) Trend in Q_{net} based on JRA-55 during 1958–2018 (°C/month/decade). (d) Similar to (c) but for latent heat flux Q_{LH}. Stippling in (a) and (b) marks regions where 4 out of 5 models agree on the sign of the trend. Stippling in (c) and (d) marks regions where trend is significant at the 95% level based on the two-tailed Student's *t* test.

6. Conclusion and discussion

In this study, we show that the distinctive cooling trend of the tropical Pacific cold tongue arises in ORAS5 not from physical processes but from a reduction in the surface flux adjustment imposed during assimilation. This adjustment, introduced to compensate for the cold tongue SST bias in the ocean model underlying ORAS5, a bias also common to CMIP6 and OMIP models, reflects the inability of current reanalysis systems to reproduce the observed long-term trends in the tropical Pacific in response to anthropogenic forcing with realistic physics. Heat budget analyses based on oceanic reanalysis data (ORAS5) and atmospheric reanalysis data (ERA5) show that, in the climatological mean, as expected, net surface heat flux contributes to surface layer warming, while ocean dynamical advective and mixing processes induce cooling in the central-to-eastern equatorial Pacific. However, comparing the climatological net surface heat flux expected given the observed SST (ERA Q_{net}) with the flux required for the ocean model to match this SST (ORAS5 Q_{net}), shows that an additional

surface flux adjustment is needed to offset excessive climatological oceanic cooling of the cold tongue. Under climate change from 1958–2024, changes in surface heat flux (from ERA5) and ocean processes (from ORAS5) both contribute positively to surface warming along the equator in the eastern Pacific. Yet the observed surface layer temperature has a cooling trend. Hence, while in the climatology the model requires a surface heat flux adjustment to correct the cold SST bias in the central-to-eastern equatorial Pacific (Fig. 1d), the observed surface layer cooling trend is produced via a reduction in this artificial flux term, a *deus ex machina* within the reanalysis framework.

The reduced need for cold tongue bias adjustment could result from improved constraints in reanalysis data in recent decades due to the availability of more and higher-quality observations. Another hypothesis is that the reduction in the adjustment term reflects compensation for SST warming in response to radiative forcing that is common in wind-driven ocean models and coupled climate models in recent periods (Figs. 1a,b and 2a,b) and, we suspect, in the ocean model underlying the ocean reanalysis data. Both explanations may be true, and may jointly contribute to the pronounced *deus ex machina* decrease over time in the surface flux adjustment. Notably, both suggest that during the earlier period (P1), the ocean model behaves more like a free-running simulation with limited observational constraints, thus requiring substantial heat flux adjustments to match observed SST due to model biases. The distinction is that the analysis increment argument posits that, in the later period (P2), more effective data assimilation tightly constrains the model through analysis increments, reducing the need for additional flux adjustment. In contrast, the alternative hypothesis suggests that, in P2, an excessive warming response to radiative forcing may compensate for the mean state bias in the equatorial Pacific cold tongue.

Validating either hypothesis remains challenging. Confirming the first would require a detailed examination of analysis increments over time, but such data are not typically available in standard ocean reanalysis outputs. For the second hypothesis, the root causes of the cold tongue mean state bias and the mechanisms underlying models' biased responses to radiative forcing remain unresolved. The need for heat flux adjustments in ocean reanalyses, together with persistent temperature biases in ocean-only GCM simulations, indicates that deficiencies persist within ocean models themselves, in addition to the well-documented surface and atmospheric biases (e.g., Seager et al. 2019). In the equatorial Pacific, many models continue to misrepresent the strength of the equatorial undercurrent (Karnauskas et al. 2020) and upwelling (Karnauskas 2025), and still struggle to accurately simulate vertical mixing (Fox-Kemper et al. 2019). In particular, models without high horizontal and vertical resolutions,

such as the NEMO model underlying ORAS5, are known to struggle to resolve small-scale current shear and fine structure of upper ocean stratification in the equatorial Pacific that are critical for mixing (Marchesiello et al. 2011; Hoteit et al. 2008; Inoue et al. 2019; Jia et al. 2021; Reichl et al. 2024). This underrepresentation has been directly linked to the cold SST bias in the equatorial Pacific and the warm bias along the South American coast (Jia et al. 2021; Reichl et al. 2024), and is likely one of the key reasons why ocean reanalyses require artificial heat flux adjustments. If so, the inferred vertical mixing warming trend along the equator in recent decades (Fig. A1c) may be an artifact of model bias, whereas in the real ocean, or in a bias-free system, such a signal might not exist. Instead, the signal of subsurface cooling is communicated into the mixed layer of the cold tongue and offsets radiatively-driven warming. Nevertheless, without a widely accepted observational benchmark, it remains difficult to fully assess the accuracy of the mixing estimates presented here or to constrain the magnitude of ocean circulation near the equator. At the same time, we cannot rule out the possibility that biases in the oceanic response originate from uncertainties in atmospheric forcing data. For example, the surface wind forcing is known to exhibit large uncertainties and substantial discrepancies across datasets (Wittenberg 2004; McGregor et al. 2012), which can lead to markedly different circulation solutions in ocean models (Merrifield and Maltrud 2011).

This study motivates intensive efforts to reconcile the discrepancy between simulated and observed SST trends in the tropical Pacific through attention to equatorial oceanic processes in addition to continued attention to atmospheric sources of bias. Several caveats should also be acknowledged. While our results show that, in the eastern equatorial Pacific, mixing estimated from monthly data aligns well with the residual term derived from the ORAS5, and that the upscaling approach from daily to monthly averages appears effective in GLORYS with similar configurations (Fig. A2), it remains unclear whether this reflects true physical consistency. Validation against in-situ observations and high-resolution models is needed to rigorously test the upscaling approach across sub-daily to monthly timescales. Looking ahead, a key direction for future research is to encourage the modeling community to standardize the inclusion of mixing-related variables in outputs of Coupled Model Intercomparison Project and to identify the most representative quantities and the optimal spatial and temporal resolutions for data storage and analysis. Besides, more in-situ observations are needed especially for vertical processes in the atmosphere and ocean that help determine the surface heat fluxes and the vertical movement of heat in the ocean between the surface and thermocline (e.g., the planned Tropical Pacific Observing System Equatorial Pacific Experiment (TEPEX) field program (Kessler et al. 2021)). A combination of field experiments and long-term monitoring by buoys,

floats and gliders should provide the needed information to identify higher frequency analogs of the physical processes operating in response to radiative forcing and guide improvements to parameterized model physics. Once done, we will be better able to assess why the Pacific Climate Change pattern emerges: the cold tongue has been cooling and the zonal SST gradient has been strengthening.

Acknowledgments.

This award was supported by NSF OCE-2219829. We thank Anna Deppenmeier and Dhruv Balwada for useful conversations.

Data availability statement. The datasets used to reproduce the results of this paper are located at https://cds.climate.copernicus.eu/cdsapp#!/dataset/reanalysis-oras5?tab=overview (ORAS5 data), https://www.metoffice.gov.uk/hadobs/hadisst (HadISST data), https://cds.climate.copernicus.eu/datasets/reanalysis-era5-single-levels-monthly-means?tab=download (ERA5 data), https://rda.ucar.edu/datasets/d628001 (JRA-55 data), https://esgf-metagrid.cloud.dkrz.de/search/cmip6-dkrz/ (CMIP6 data) and https://esgf-metagrid.cloud.dkrz.de/search/cmip6-dkrz (OMIP-2).

Appendix

To demonstrate that the residual heat flux is likely dominated by vertical mixing and to diagnose its change over time, we implement a Richardson number dependent estimate of mixing. We express the contribution of vertical diffusive heat flux as an equivalent temperature tendency of the surface layer (d = 50 m) to ensure consistency with the other budget terms. The vertical diffusion term at the base of the surface layer (d = 50 m) is written as:

$$Q_{diffu} = -\frac{1}{d}(\kappa \frac{\partial T}{\partial z})\Big|_{-d} \quad \text{Eq. (A1)}$$

where κ indicates vertical eddy diffusivity. Following Pacanowski and Philander (1981), κ is parameterized as a function of the gradient Richardson number as:

$$\kappa_{Ri} = \frac{\upsilon_0}{(1+aRi)^{n+1}} + \frac{\upsilon_b}{(1+aRi)} + \kappa_b \quad \text{Eq. (A2)}$$

with $\upsilon_0 = 10^{-2}$ m^2/s, $\upsilon_b = 10^{-4}$ m^2/s, n =2; a = 5, $\kappa_b = 10^{-5}$ m^2/s. The gradient Richardson number Ri is defined as:

$$Ri = \frac{\alpha g \frac{\partial T}{\partial z}}{\left(\frac{\partial u}{\partial z}\right)^2 + \left(\frac{\partial v}{\partial z}\right)^2} \quad \text{Eq. (A3)}$$

where u and v represent the zonal and meridional currents, respectively, $\alpha = 8.75*10^{-6}*(T+6)$ ℃ and $g = 9.8$ m/s^2. A minimum value Ri is set to 0 to avoid invalid diagnostic values. It should be noted that ORAS5 actually uses a Turbulent Kinetic Energy (TKE) scheme to parameterize eddy diffusivity and vertical mixing (Bernard et al. 2006; Blanke and Delecluse 1993), instead of this simple Ri-based approach. The Ri-dependent approach is adopted here due to its practical and diagnostic utility in illustrating the roles of shear and buoyancy in driving mixing (Moum et al. 1986, 1989; Peters et al. 1988; Hayes et al. 1991; Wang and McPhaden 1999; Huang et al. 2010), especially when model outputs of mixing are unavailable for directly computing the prognostic TKE equation.

We therefore estimate the monthly κ_{Ri} at the base of the surface layer using the squared vertical shear of the horizontal currents ($(\frac{\partial u}{\partial z})^2 + (\frac{\partial v}{\partial z})^2$) and the buoyancy frequency associated with the vertical temperature gradient ($\alpha g \frac{\partial T}{\partial z}$) based on ORAS5 data. Ideally, the Richardson number should be derived from data with finer spatial and higher temporal resolution. When computed from heavily averaged in-situ data, particularly in regions of weak turbulence where the Richardson number can vary by orders of magnitude, the Richardson number and the parameterized diffusivity can be significantly biased (Peters et al. 1988; Moum et al. 1989). However, in regions with strong turbulence, such as the eastern equatorial Pacific, unstable regimes characterized by low Richardson numbers remain identifiable even in heavily averaged datasets (Moum et al. 1986; Pham et al. 2017). In terms of spatial resolution, strong turbulent regions near the equator can be resolved with vertical bin sizes of approximately 10–20 m (Zaron and Moum 2009; Smyth and Moum 2013), comparable to the typical vertical resolution of ocean models such as NEMO. In terms of temporal resolution, Richardson numbers in strongly turbulent equatorial regions computed from daily-averaged data are generally consistent with those derived from hourly observations (Pham et al. 2017). Furthermore, previous studies documented the seasonal evolution of upper ocean mixing and its modulation by El Niño and La Niña events, which exhibit limited submonthly variability at 0°, 140°W (Moum et al. 2013; Pham et al. 2017). Therefore, we assume that temporal averaging does not substantially alter the analysis of the dynamics of vertical mixing in the eastern equatorial Pacific, and that the parameterization is suitable for upscaling. This assumption reasonably requires that the covariance between sub-monthly variability in eddy diffusivity and the vertical

temperature gradient is smaller than the monthly covariance at the ~10 m vertical resolution scale (Zaron and Moum 2009).

Under this assumption, we estimate the climatological vertical diffusion in P1 using the monthly temperature gradient and eddy diffusivity inferred from monthly Richardson numbers (Fig. A1). The resulting diffusion term Q_{diffu} roughly captures the spatial pattern of the residual term Q_{res} (Fig. 3c). In Figure A1d, we show the seasonal cycle of κ_{Ri} at the base of the surface layer along the equator based on the climatological mean for each calendar month. The magnitude of κ_{Ri} varies significantly along the equator, with values around 10^{-4} m^2/s in the central-to-eastern Pacific (180°~110°W), peaking at 10^{-3} m^2/s near 140°W. The inferred diffusivity exhibits a pronounced seasonal cycle with stronger values during boreal autumn and winter and weaker values in spring and summer (Fig. A1d), which, as noted before, is primarily driven by the strong seasonal variations in the vertical temperature gradient and shear squared in the cold tongue region (Moum et al. 2013). Assuming the vertical diffusion dominates the residual term, we can also estimate the mean eddy diffusivity in P1 based on the climatological Q_{res} as:

$$\kappa_{res} = \frac{Q_{res}}{\frac{\partial T}{\partial z}} \qquad \text{Eq. (A4)}$$

in which $\frac{\partial T}{\partial z}$ is calculated as the climatological temperature gradient during P1 at the depth of 50 m based on ORAS5. In Figure A1e, we show the seasonal evolution of this equatorial eddy diffusivity inferred from the residual. The strong resemblance between κ_{res} and κ_{Ri} (Fig. A1d,e) lends further support to our assumption that vertical diffusion is the primary contributor to the residual term.

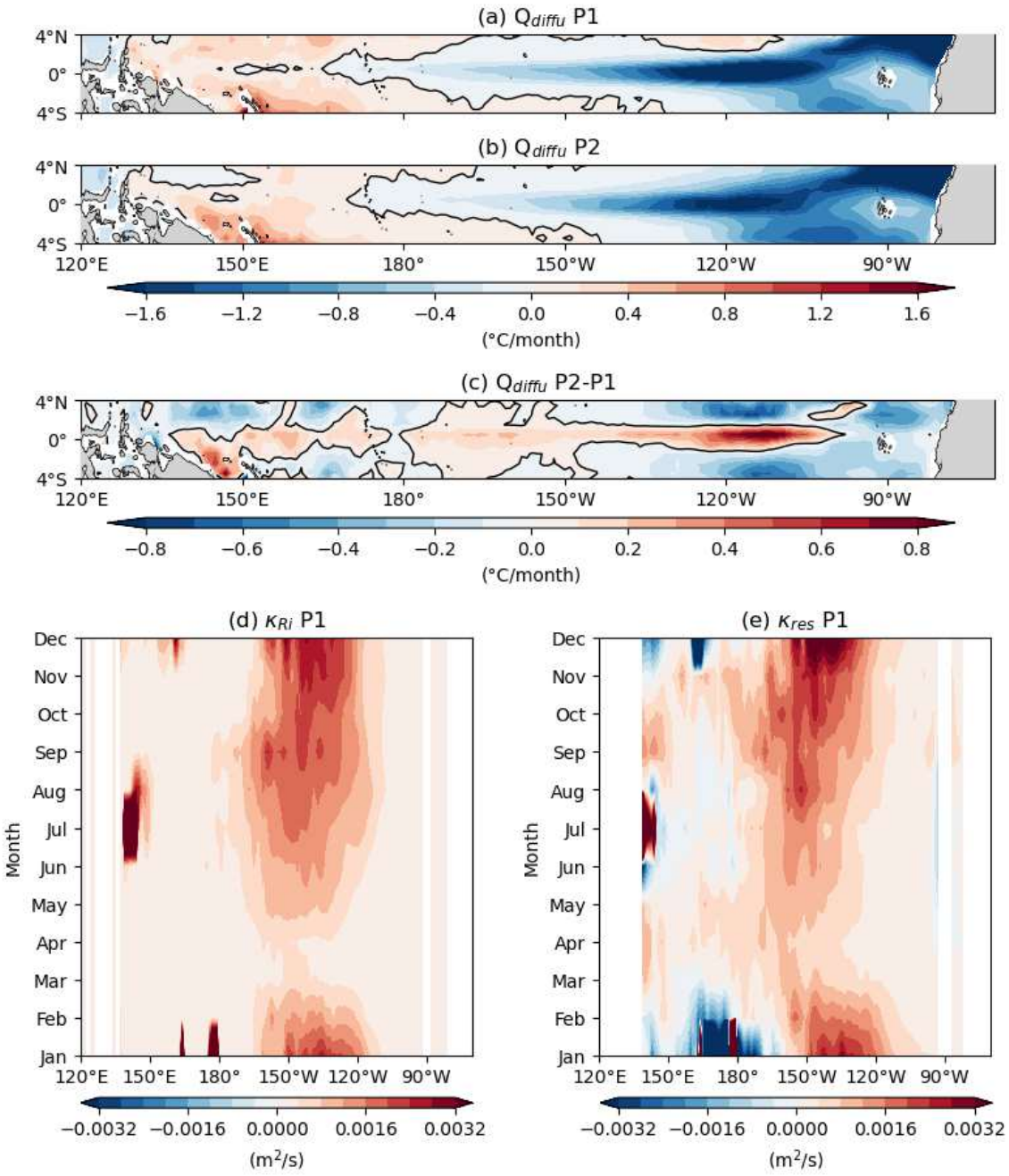

Figure A1. Climatological vertical diffusion Q_{diffu} at the base of the surface layer (°C/month) estimated using Eq. (A1) for (a) P1 (1958–1977) and (b) P2 (2005–2024) . (c) Difference in Q_{diffu} (°C/month) between P2 and P1. Seasonal evolution of κ along the equator (m^2/s) in P1, estimated from (d) Richardson number (κ_{Ri}) and (e) residual term Q_{res} (κ_{res}) in P1.

Similarly, we calculate the Ri-based eddy diffusivity in P2 and estimate the corresponding diffusion term in Figure A1b. As shown in Figure A1c, the change in the Ri-based diffusion term Q_{diffu} corresponds to surface layer warming along the equator. At the equator, this warming change is quantitatively consistent with the residual-based estimates (Fig. 3f). The differences between inferred mixing and the residual term observed in the off-equatorial

regions indicate that other processes such as changes in the analysis increment and horizontal mixing also contribute to changes in the residual term.

The upscaling approach used to quantify mixing based on monthly outputs requires further validation. Previous studies have shown that Richardson numbers derived from daily-averaged data in strongly turbulent equatorial regions are broadly consistent with those from higher-frequency data (Pham et al. 2017). Since ORAS5 provides only monthly outputs, we used daily subsurface temperature and current data from GLORYS to test whether this consistency also holds when comparing daily to monthly averages. GLORYS uses essentially the same configuration and boundary forcing as ORAS5 but at higher horizontal resolution and with daily outputs during 1993–2024. As shown in Figure A2, the marginally unstable regime for vertical mixing in the equatorial Pacific is captured reasonably consistently across daily and monthly-averaged GLORYS data and monthly ORAS5 over their overlapping period (1993–2024). Nevertheless, the extent to which *Ri*-based parameterizations accurately represent real-world mixing remains uncertain. Ocean mixing can also be driven by finer-scale wave dynamics that are unresolved at the current vertical resolution (Jia et al. 2020) and lie beyond what large-scale Ri fields can capture.

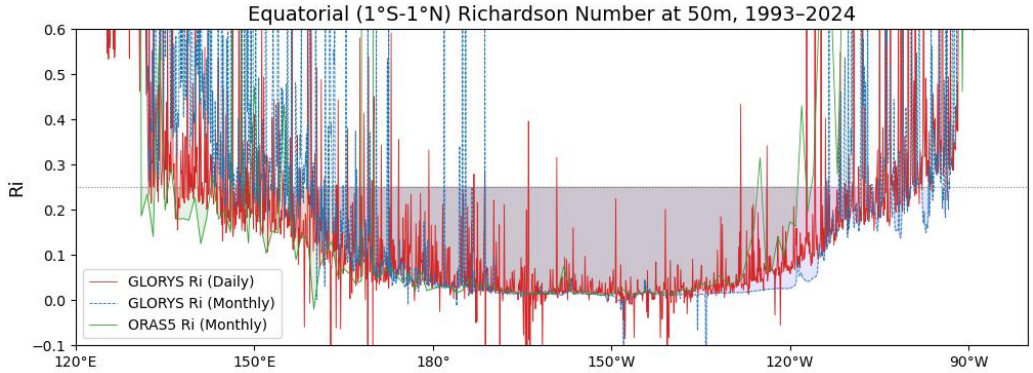

Figure A2. Equatorial (1°S–1°N) distribution of the Richardson number at 50 m, calculated from daily GLORYS data (red), monthly-averaged GLORYS data (blue), and monthly ORAS5 data (green). Shadings indicate regions of mixing instability as identified from each dataset, and the dashed line marks the critical threshold of $Ri = 0.25$.

598 REFERENCES

599 Andrews, T., and Coauthors, 2022: On the Effect of Historical SST Patterns on Radiative
600 Feedback. *JGR Atmospheres*, **127**, e2022JD036675,
601 https://doi.org/10.1029/2022JD036675.

602 Armour, K. C., and Coauthors, 2024: Sea-surface temperature pattern effects have slowed
603 global warming and biased warming-based constraints on climate sensitivity. *Proc.*
604 *Natl. Acad. Sci. U.S.A.*, **121**, e2312093121, https://doi.org/10.1073/pnas.2312093121.

605 Balmaseda, M. A., K. Mogensen, and A. T. Weaver, 2013: Evaluation of the ECMWF ocean
606 reanalysis system ORAS4. *Quart J Royal Meteoro Soc*, **139**, 1132–1161,
607 https://doi.org/10.1002/qj.2063.

608 Balmaseda, M. A., and Coauthors, 2015: The Ocean Reanalyses Intercomparison Project
609 (ORA-IP). *Journal of Operational Oceanography*, **8**, s80–s97,
610 https://doi.org/10.1080/1755876X.2015.1022329.

611 Bentamy, A., and Coauthors, 2017: Review and assessment of latent and sensible heat flux
612 accuracy over the global oceans. *Remote Sensing of Environment*, **201**, 196–218,
613 https://doi.org/10.1016/j.rse.2017.08.016.

614 Bernard, B., and Coauthors, 2006: Impact of partial steps and momentum advection schemes
615 in a global ocean circulation model at eddy-permitting resolution. *Ocean Dynamics*,
616 **56**, 543–567, https://doi.org/10.1007/s10236-006-0082-1.

617 Berry, D. I., and E. C. Kent, 2009: A New Air–Sea Interaction Gridded Dataset from
618 ICOADS With Uncertainty Estimates. *Bull. Amer. Meteor. Soc.*, **90**, 645–656,
619 https://doi.org/10.1175/2008BAMS2639.1.

620 Betts, A. K., and W. Ridgway, 1989: Climatic Equilibrium of the Atmospheric Convective
621 Boundary Layer over a Tropical Ocean. *J. Atmos. Sci.*, **46**, 2621–2641,
622 https://doi.org/10.1175/1520-0469(1989)046<2621:CEOTAC>2.0.CO;2.

623 Blanke, B., and P. Delecluse, 1993: Variability of the Tropical Atlantic Ocean Simulated by a
624 General Circulation Model with Two Different Mixed-Layer Physics. *J. Phys.*
625 *Oceanogr.*, **23**, 1363–1388, https://doi.org/10.1175/1520-
626 0485(1993)023<1363:VOTTAO>2.0.CO;2.

627 Bretherton, C. S., 1993: Understanding Albrecht's Model of Trade Cumulus Cloud Fields. *J.*
628 *Atmos. Sci.*, **50**, 2264–2283, https://doi.org/10.1175/1520-
629 0469(1993)050<2264:UAMOTC>2.0.CO;2.

630 Browne, P. A., P. De Rosnay, H. Zuo, A. Bennett, and A. Dawson, 2019: Weakly Coupled
631 Ocean–Atmosphere Data Assimilation in the ECMWF NWP System. *Remote*
632 *Sensing*, **11**, 234, https://doi.org/10.3390/rs11030234.

633 Brunke, M. A., C. W. Fairall, X. Zeng, L. Eymard, and J. A. Curry, 2003: Which Bulk
634 Aerodynamic Algorithms are Least Problematic in Computing Ocean Surface
635 Turbulent Fluxes? *J. Climate*, **16**, 619–635, https://doi.org/10.1175/1520-
636 0442(2003)016<0619:WBAAAL>2.0.CO;2.

637 Byrne, H., R. Seager, and J. E. Smerdon, 2025: CMIP6 models cannot capture long-term
638 forced changes in the tropical Pacific sea surface temperature gradient. *Nat Commun*,
639 https://doi.org/10.1038/s41467-025-66839-w.

640 Coats, S., and K. B. Karnauskas, 2017: Are Simulated and Observed Twentieth Century
641 Tropical Pacific Sea Surface Temperature Trends Significant Relative to Internal
642 Variability? *Geophysical Research Letters*, **44**, 9928–9937,
643 https://doi.org/10.1002/2017GL074622.

644 Dee, D. P., and Coauthors, 2011: The ERA-Interim reanalysis: configuration and
645 performance of the data assimilation system. *Quart J Royal Meteoro Soc*, **137**, 553–
646 597, https://doi.org/10.1002/qj.828.

647 Deppenmeier, A.-L., F. O. Bryan, W. S. Kessler, and L. Thompson, 2022: Diabatic
648 Upwelling in the Tropical Pacific: Seasonal and Subseasonal Variability. *Journal of*
649 *Physical Oceanography*, **52**, 2657–2668, https://doi.org/10.1175/JPO-D-21-0316.1.

650 Dhame, S., D. Olonscheck, and M. Rugenstein, 2025: Higher-Resolution Climate Models Do
651 Not Consistently Reproduce the Observed Tropical Pacific Warming Pattern. *Journal*
652 *of Climate*, **38**, 3131–3149, https://doi.org/10.1175/JCLI-D-24-0248.1.

653 Dong, L., and T. Zhou, 2014: The formation of the recent cooling in the eastern tropical
654 Pacific Ocean and the associated climate impacts: A competition of global warming,
655 IPO, and AMO. *JGR Atmospheres*, **119**, https://doi.org/10.1002/2013JD021395.

656 Eyring, V., S. Bony, G. A. Meehl, C. A. Senior, B. Stevens, R. J. Stouffer, and K. E. Taylor,
657 2016: Overview of the Coupled Model Intercomparison Project Phase 6 (CMIP6)
658 experimental design and organization. *Geosci. Model Dev.*, **9**, 1937–1958,
659 https://doi.org/10.5194/gmd-9-1937-2016.

660 Fox-Kemper, B., and Coauthors, 2019: Challenges and Prospects in Ocean Circulation
661 Models. *Front. Mar. Sci.*, **6**, 65, https://doi.org/10.3389/fmars.2019.00065.

662 Gregory, J. M., and T. Andrews, 2016: Variation in climate sensitivity and feedback
663 parameters during the historical period. *Geophysical Research Letters*, **43**, 3911–
664 3920, https://doi.org/10.1002/2016GL068406.

665 Griffies, S. M., and Coauthors, 2016: OMIP contribution to CMIP6: experimental and
666 diagnosticprotocol for the physical component of the Ocean Model Intercomparison
667 Project. *Geosci. Model Dev.*, **9**, 3231–3296, https://doi.org/10.5194/gmd-9-3231-
668 2016.

669 Gulev, S., T. Jung, and E. Ruprecht, 2007: Estimation of the Impact of Sampling Errors in the
670 VOS Observations on Air–Sea Fluxes. Part II: Impact on Trends and Interannual
671 Variability. *Journal of Climate*, **20**, 302–315, https://doi.org/10.1175/JCLI4008.1.

672 Hayes, S. P., P. Chang, and M. J. McPhaden, 1991: Variability of the sea surface temperature
673 in the eastern equatorial Pacific during 1986–1988. *J. Geophys. Res.*, **96**, 10553–
674 10566, https://doi.org/10.1029/91JC00942.

675 Hersbach, H., and Coauthors, 2020: The ERA5 global reanalysis. *Quart J Royal Meteoro*
676 *Soc*, **146**, 1999–2049, https://doi.org/10.1002/qj.3803.

677 Holmes, R. M., J. D. Zika, and M. H. England, 2019: Diathermal Heat Transport in a Global
678 Ocean Model. *Journal of Physical Oceanography*, **49**, 141–161,
679 https://doi.org/10.1175/JPO-D-18-0098.1.

680 Hoteit, I., B. Cornuelle, V. Thierry, and D. Stammer, 2008: Impact of Resolution and
681 Optimized ECCO Forcing on Simulations of the Tropical Pacific. *Journal of*
682 *Atmospheric and Oceanic Technology*, **25**, 131–147,
683 https://doi.org/10.1175/2007JTECHO528.1.

684 Huang, B., Y. Xue, D. Zhang, A. Kumar, and M. J. McPhaden, 2010: The NCEP GODAS
685 Ocean Analysis of the Tropical Pacific Mixed Layer Heat Budget on Seasonal to
686 Interannual Time Scales. *Journal of Climate*, **23**, 4901–4925,
687 https://doi.org/10.1175/2010JCLI3373.1.

688 Inoue, R., R. Lien, J. N. Moum, R. C. Perez, and M. C. Gregg, 2019: Variations of Equatorial
689 Shear, Stratification, and Turbulence Within a Tropical Instability Wave Cycle. *JGR*
690 *Oceans*, **124**, 1858–1875, https://doi.org/10.1029/2018JC014480.

691 Isemer, H.-J., J. Willebrand, and L. Hasse, 1989: Fine Adjustment of Large Scale Air-Sea
692 Energy Flux Parameterizations by Direct Estimates of Ocean Heat Transport. *J.*
693 *Climate*, **2**, 1173–1184, https://doi.org/10.1175/1520-
694 0442(1989)002<1173:FAOLSA>2.0.CO;2.

695 Jia, Y., K. J. Richards, and H. Annamalai, 2021: The impact of vertical resolution in reducing
696 biases in sea surface temperature in a tropical Pacific Ocean model. *Ocean Modelling*,
697 **157**, 101722, https://doi.org/10.1016/j.ocemod.2020.101722.

698 Jiang, F., R. Seager, and M. A. Cane, 2024a: A climate change signal in the tropical Pacific
699 emerges from decadal variability. *Nat Commun*, **15**, 8291,
700 https://doi.org/10.1038/s41467-024-52731-6.

701 ——, ——, and ——, 2024b: Historical Subsurface Cooling in the Tropical Pacific and its
702 Dynamics. *Journal of Climate*, https://doi.org/10.1175/JCLI-D-24-0007.1.

703 ——, ——, ——, C. Karamperidou, and N. G. Brizuela, 2025: Subsurface Cooling and Sea
704 Surface Temperature Pattern Formation Over the Equatorial Pacific. *JGR Oceans*,
705 **130**, e2024JC022222, https://doi.org/10.1029/2024JC022222.

706 Josey, S. A., E. C. Kent, and P. K. Taylor, 1999: New Insights into the Ocean Heat Budget
707 Closure Problem from Analysis of the SOC Air–Sea Flux Climatology. *J. Climate*,
708 **12**, 2856–2880, https://doi.org/10.1175/1520-
709 0442(1999)012<2856:NIITOH>2.0.CO;2.

710 Karnauskas, K. B., 2025: How Fast is the Mean Upwelling in the Equatorial Pacific Ocean?
711 *Journal of Climate*, https://doi.org/10.1175/JCLI-D-24-0704.1.

712 ——, J. Jakoboski, T. M. S. Johnston, W. B. Owens, D. L. Rudnick, and R. E. Todd, 2020:
713 The Pacific Equatorial Undercurrent in Three Generations of Global Climate Models
714 and Glider Observations. *JGR Oceans*, **125**, e2020JC016609,
715 https://doi.org/10.1029/2020JC016609.

716 Kessler, W. S., S. Cravatte, P. G. Strutton, A. J. Sutton, A. Kumar, and Y. Takaya, 2021:
717 Final report of TPOS 2020 (Tech. Rep. No. 268). UNESCO IOC Global Ocean
718 Observing System (GOOS).

719 Kim, H., S. M. Kang, J. E. Kay, and S.-P. Xie, 2022: Subtropical clouds key to Southern
720 Ocean teleconnections to the tropical Pacific. *Proc. Natl. Acad. Sci. U.S.A.*, **119**,
721 e2200514119, https://doi.org/10.1073/pnas.2200514119.

722 Kobayashi, S., and Coauthors, 2015: The JRA-55 Reanalysis: General Specifications and
723 Basic Characteristics. *Journal of the Meteorological Society of Japan*, **93**, 5–48,
724 https://doi.org/10.2151/jmsj.2015-001.

725 Large, W. G., and S. G. Yeager, 2009: The global climatology of an interannually varying
726 air–sea flux data set. *Clim Dyn*, **33**, 341–364, https://doi.org/10.1007/s00382-008-
727 0441-3.

728 Large, W. G., G. Danabasoglu, S. C. Doney, and J. C. McWilliams, 1997: Sensitivity to
729 Surface Forcing and Boundary Layer Mixing in a Global Ocean Model: Annual-Mean
730 Climatology. *J. Phys. Oceanogr.*, **27**, 2418–2447, https://doi.org/10.1175/1520-
731 0485(1997)027<2418:STSFAB>2.0.CO;2.

732 Lee, S., M. L'Heureux, A. T. Wittenberg, R. Seager, P. A. O'Gorman, and N. C. Johnson,
733 2022: On the future zonal contrasts of equatorial Pacific climate: Perspectives from
734 Observations, Simulations, and Theories. *npj Clim Atmos Sci*, **5**, 82,
735 https://doi.org/10.1038/s41612-022-00301-2.

736 Lellouche, J.-M., and Coauthors, 2021: The Copernicus Global 1/12° Oceanic and Sea Ice
737 GLORYS12 Reanalysis. *Front. Earth Sci.*, **9**, 698876,
738 https://doi.org/10.3389/feart.2021.698876.

739 L'Heureux, M. L., M. K. Tippett, and W. Wang, 2022: Prediction Challenges From Errors in
740 Tropical Pacific Sea Surface Temperature Trends. *Front. Clim.*, **4**, 837483,
741 https://doi.org/10.3389/fclim.2022.837483.

742 Li, G., and S.-P. Xie, 2014: Tropical Biases in CMIP5 Multimodel Ensemble: The Excessive
743 Equatorial Pacific Cold Tongue and Double ITCZ Problems*. *Journal of Climate*, **27**,
744 1765–1780, https://doi.org/10.1175/JCLI-D-13-00337.1.

745 ——, B. Ren, C. Yang, and J. Zheng, 2011: Revisiting the trend of the tropical and
746 subtropical Pacific surface latent heat flux during 1977–2006. *J. Geophys. Res.*, **116**,
747 D10115, https://doi.org/10.1029/2010JD015444.

748 Liu, C., and Coauthors, 2017: Evaluation of satellite and reanalysis-based global net surface
749 energy flux and uncertainty estimates. *JGR Atmospheres*, **122**, 6250–6272,
750 https://doi.org/10.1002/2017JD026616.

751 Liu, C., F. Wang, A. Köhl, X. Wang, C. Wang, and K. J. Richards, 2025: Subsurface ocean
752 turbulent mixing enhances central Pacific ENSO. *Nat Commun*, **16**, 2315,
753 https://doi.org/10.1038/s41467-025-57058-4.

754 Liu, J., and J. A. Curry, 2006: Variability of the tropical and subtropical ocean surface latent
755 heat flux during 1989–2000. *Geophysical Research Letters*, **33**, 2005GL024809,
756 https://doi.org/10.1029/2005GL024809.

757 Liu, Z., S. Vavrus, F. He, N. Wen, and Y. Zhong, 2005: Rethinking Tropical Ocean Response
758 to Global Warming: The Enhanced Equatorial Warming*. *Journal of Climate*, **18**,
759 4684–4700, https://doi.org/10.1175/JCLI3579.1.

760 Luo, J.-J., G. Wang, and D. Dommenget, 2018: May common model biases reduce CMIP5's
761 ability to simulate the recent Pacific La Niña-like cooling? *Clim Dyn*, **50**, 1335–1351,
762 https://doi.org/10.1007/s00382-017-3688-8.

763 Marchesiello, P., X. Capet, C. Menkes, and S. C. Kennan, 2011: Submesoscale dynamics in
764 tropical instability waves. *Ocean Modelling*, **39**, 31–46,
765 https://doi.org/10.1016/j.ocemod.2011.04.011.

766 McGregor, S., A. S. Gupta, and M. H. England, 2012: Constraining Wind Stress Products
767 with Sea Surface Height Observations and Implications for Pacific Ocean Sea Level
768 Trend Attribution. *Journal of Climate*, **25**, 8164–8176, https://doi.org/10.1175/JCLI-
769 D-12-00105.1.

770 Meehl, G. A., A. Hu, B. D. Santer, and S.-P. Xie, 2016: Contribution of the Interdecadal
771 Pacific Oscillation to twentieth-century global surface temperature trends. *Nature*
772 *Clim Change*, **6**, 1005–1008, https://doi.org/10.1038/nclimate3107.

773 Merrifield, M. A., and M. E. Maltrud, 2011: Regional sea level trends due to a Pacific trade
774 wind intensification: SEA LEVEL AND PACIFIC TRADE WINDS. *Geophys. Res.*
775 *Lett.*, **38**, n/a-n/a, https://doi.org/10.1029/2011GL049576.

776 Moum, J. N., T. R. Osborn, and W. R. Crawford, 1986: Pacific Equatorial Turbulence:
777 Revisited. *J. Phys. Oceanogr.*, **16**, 1516–1522, https://doi.org/10.1175/1520-
778 0485(1986)016<1516:PETR>2.0.CO;2.

779 Moum, J. N., D. R. Caldwell, and C. A. Paulson, 1989: Mixing in the equatorial surface layer
780 and thermocline. *J. Geophys. Res.*, **94**, 2005–2022,
781 https://doi.org/10.1029/JC094iC02p02005.

782 Moum, J. N., R.-C. Lien, A. Perlin, J. D. Nash, M. C. Gregg, and P. J. Wiles, 2009: Sea
783 surface cooling at the Equator by subsurface mixing in tropical instability waves.
784 *Nature Geosci*, **2**, 761–765, https://doi.org/10.1038/ngeo657.

785 Moum, J. N., A. Perlin, J. D. Nash, and M. J. McPhaden, 2013: Seasonal sea surface cooling
786 in the equatorial Pacific cold tongue controlled by ocean mixing. *Nature*, **500**, 64–67,
787 https://doi.org/10.1038/nature12363.

788 Nakamura, K., S. Kido, T. Ijichi, and T. Tozuka, 2024: Generation Mechanisms of SST
789 Anomalies Associated with the Canonical El Niño Focusing on Vertical Mixing.
790 *Journal of Climate*, **37**, 3593–3612, https://doi.org/10.1175/JCLI-D-23-0288.1.

791 O'Neill, B. C., and Coauthors, 2016: The Scenario Model Intercomparison Project
792 (ScenarioMIP) for CMIP6. *Geosci. Model Dev.*, **9**, 3461–3482,
793 https://doi.org/10.5194/gmd-9-3461-2016.

794 Pacanowski, R. C., and S. G. H. Philander, 1981: Parameterization of Vertical Mixing in
795 Numerical Models of Tropical Oceans. *J. Phys. Oceanogr.*, **11**, 1443–1451,
796 https://doi.org/10.1175/1520-0485(1981)011<1443:POVMIN>2.0.CO;2.

797 Peters, H., M. C. Gregg, and J. M. Toole, 1988: On the parameterization of equatorial
798 turbulence. *J. Geophys. Res.*, **93**, 1199–1218,
799 https://doi.org/10.1029/JC093iC02p01199.

800 Pham, H. T., W. D. Smyth, S. Sarkar, and J. N. Moum, 2017: Seasonality of Deep Cycle
801 Turbulence in the Eastern Equatorial Pacific. *Journal of Physical Oceanography*, **47**,
802 2189–2209, https://doi.org/10.1175/JPO-D-17-0008.1.

803 Pillai, P. A., S. A. Rao, A. Srivastava, D. A. Ramu, M. Pradhan, and R. S. Das, 2021: Impact
804 of the tropical Pacific SST biases on the simulation and prediction of Indian summer
805 monsoon rainfall in CFSv2, ECMWF-System4, and NMME models. *Clim Dyn*, **56**,
806 1699–1715, https://doi.org/10.1007/s00382-020-05555-1.

807 Rahul, S., and C. Gnanaseelan, 2013: Net Heat Flux Over the Indian Ocean: Trends, Driving
808 Mechanisms, and Uncertainties. *IEEE Geosci. Remote Sensing Lett.*, **10**, 776–780,
809 https://doi.org/10.1109/LGRS.2012.2223194.

810 Ray, S., A. T. Wittenberg, S. M. Griffies, and F. Zeng, 2018a: Understanding the Equatorial
811 Pacific Cold Tongue Time-Mean Heat Budget. Part I: Diagnostic Framework. *J.*
812 *Climate*, **31**, 9965–9985, https://doi.org/10.1175/JCLI-D-18-0152.1.

813 ——, ——, ——, and ——, 2018b: Understanding the Equatorial Pacific Cold Tongue
814 Time-Mean Heat Budget. Part II: Evaluation of the GFDL-FLOR Coupled GCM. *J.*
815 *Climate*, **31**, 9987–10011, https://doi.org/10.1175/JCLI-D-18-0153.1.

816 Rayner, N. A., D. E. Parker, E. B. Horton, C. K. Folland, L. V. Alexander, D. P. Rowell, E.
817 C. Kent, and A. Kaplan, 2003: Global analyses of sea surface temperature, sea ice,
818 and night marine air temperature since the late nineteenth century. *J. Geophys. Res.*,
819 **108**, 2002JD002670, https://doi.org/10.1029/2002JD002670.

820 Reichl, B. G., A. T. Wittenberg, S. M. Griffies, and A. Adcroft, 2024: Improving Equatorial
821 Upper Ocean Vertical Mixing in the NOAA/GFDL OM4 Model. *Earth and Space*
822 *Science*, **11**, e2023EA003485, https://doi.org/10.1029/2023EA003485.

823 Rienecker, M. M., and Coauthors, 2011: MERRA: NASA's Modern-Era Retrospective
824 Analysis for Research and Applications. *Journal of Climate*, **24**, 3624–3648,
825 https://doi.org/10.1175/JCLI-D-11-00015.1.

826 Rose, B. E. J., K. C. Armour, D. S. Battisti, N. Feldl, and D. D. B. Koll, 2014: The
827 dependence of transient climate sensitivity and radiative feedbacks on the spatial
828 pattern of ocean heat uptake. *Geophysical Research Letters*, **41**, 1071–1078,
829 https://doi.org/10.1002/2013GL058955.

830 Rugenstein, M., S. Dhame, D. Olonscheck, R. J. Wills, M. Watanabe, and R. Seager, 2023:
831 Connecting the SST Pattern Problem and the Hot Model Problem. *Geophysical*
832 *Research Letters*, **50**, e2023GL105488, https://doi.org/10.1029/2023GL105488.

Seager, R., M. B. Blumenthal, and Y. Kushnir, 1995: An Advective Atmospheric Mixed Layer Model for Ocean Modeling Purposes: Global Simulation of Surface Heat Fluxes. *J. Climate*, **8**, 1951–1964, https://doi.org/10.1175/1520-0442(1995)008<1951:AAAMLM>2.0.CO;2.

——, M. Cane, N. Henderson, D.-E. Lee, R. Abernathey, and H. Zhang, 2019: Strengthening tropical Pacific zonal sea surface temperature gradient consistent with rising greenhouse gases. *Nat. Clim. Chang.*, **9**, 517–522, https://doi.org/10.1038/s41558-019-0505-x.

——, N. Henderson, and M. Cane, 2022: Persistent Discrepancies between Observed and Modeled Trends in the Tropical Pacific Ocean. *Journal of Climate*, **35**, 4571–4584, https://doi.org/10.1175/JCLI-D-21-0648.1.

——, M. Ting, P. Alexander, H. Liu, J. Nakamura, C. Li, and M. Newman, 2023: Ocean-forcing of cool season precipitation drives ongoing and future decadal drought in southwestern North America. *npj Clim Atmos Sci*, **6**, 141, https://doi.org/10.1038/s41612-023-00461-9.

Simpson, I. R., and Coauthors, 2025: Confronting Earth System Model trends with observations. *Sci. Adv.*, **11**, eadt8035, https://doi.org/10.1126/sciadv.adt8035.

Smyth, W. D., and J. N. Moum, 2013: Marginal instability and deep cycle turbulence in the eastern equatorial Pacific Ocean. *Geophysical Research Letters*, **40**, 6181–6185, https://doi.org/10.1002/2013GL058403.

Sobel, A. H., and Coauthors, 2023: Near-term tropical cyclone risk and coupled Earth system model biases. *Proc. Natl. Acad. Sci. U.S.A.*, **120**, e2209631120, https://doi.org/10.1073/pnas.2209631120.

Solomon, A., and M. Newman, 2012: Reconciling disparate twentieth-century Indo-Pacific ocean temperature trends in the instrumental record. *Nature Clim Change*, **2**, 691–699, https://doi.org/10.1038/nclimate1591.

Tang, R., Y. Wang, Y. Jiang, M. Liu, Z. Peng, Y. Hu, L. Huang, and Z.-L. Li, 2024: A review of global products of air-sea turbulent heat flux: accuracy, mean, variability, and trend. *Earth-Science Reviews*, **249**, 104662, https://doi.org/10.1016/j.earscirev.2023.104662.

Tozuka, T., 2025: Importance of the vertical mixing process in the development of El Niño Modoki. *npj Clim Atmos Sci*, **8**, 76, https://doi.org/10.1038/s41612-025-00973-6.

Tsujino, H., and Coauthors, 2018: JRA-55 based surface dataset for driving ocean–sea-ice models (JRA55-do). *Ocean Modelling*, **130**, 79–139, https://doi.org/10.1016/j.ocemod.2018.07.002.

——, and Coauthors, 2020: Evaluation of global ocean–sea-ice model simulations based on the experimental protocols of the Ocean Model Intercomparison Project phase 2 (OMIP-2). *Geosci. Model Dev.*, **13**, 3643–3708, https://doi.org/10.5194/gmd-13-3643-2020.

872 Valdivieso, M., and Coauthors, 2017: An assessment of air–sea heat fluxes from ocean and
873 coupled reanalyses. *Clim Dyn*, **49**, 983–1008, https://doi.org/10.1007/s00382-015-
874 2843-3.

875 Vidard, A., P.-A. Bouttier, and F. Vigilant, 2015: NEMOTAM: tangent and adjoint models
876 for the ocean modelling platform NEMO. *Geosci. Model Dev.*, **8**, 1245–1257,
877 https://doi.org/10.5194/gmd-8-1245-2015.

878 Wang, W., and M. J. McPhaden, 1999: The Surface-Layer Heat Balance in the Equatorial
879 Pacific Ocean. Part I: Mean Seasonal Cycle*. *J. Phys. Oceanogr.*, **29**, 1812–1831,
880 https://doi.org/10.1175/1520-0485(1999)029<1812:TSLHBI>2.0.CO;2.

881 Warner, S. J., and J. N. Moum, 2019: Feedback of Mixing to ENSO Phase Change.
882 *Geophysical Research Letters*, **46**, 13920–13927,
883 https://doi.org/10.1029/2019GL085415.

884 Watanabe, M., J.-L. Dufresne, Y. Kosaka, T. Mauritsen, and H. Tatebe, 2021: Enhanced
885 warming constrained by past trends in equatorial Pacific sea surface temperature
886 gradient. *Nat. Clim. Chang.*, **11**, 33–37, https://doi.org/10.1038/s41558-020-00933-3.

887 ——, S. M. Kang, M. Collins, Y.-T. Hwang, S. McGregor, and M. F. Stuecker, 2024:
888 Possible shift in controls of the tropical Pacific surface warming pattern. *Nature*, **630**,
889 315–324, https://doi.org/10.1038/s41586-024-07452-7.

890 Wills, R. C. J., Y. Dong, C. Proistosecu, K. C. Armour, and D. S. Battisti, 2022: Systematic
891 Climate Model Biases in the Large-Scale Patterns of Recent Sea-Surface Temperature
892 and Sea-Level Pressure Change. *Geophysical Research Letters*, **49**, e2022GL100011,
893 https://doi.org/10.1029/2022GL100011.

894 Wittenberg, A. T., 2004: Extended Wind Stress Analyses for ENSO. *J. Climate*, **17**, 2526–
895 2540, https://doi.org/10.1175/1520-0442(2004)017<2526:EWSAFE>2.0.CO;2.

896 ——, and Coauthors, 2018: Improved Simulations of Tropical Pacific Annual-Mean Climate
897 in the GFDL FLOR and HiFLOR Coupled GCMs. *J Adv Model Earth Syst*, **10**, 3176–
898 3220, https://doi.org/10.1029/2018MS001372.

899 Yang, C., B. S. Giese, and L. Wu, 2014: Ocean dynamics and tropical Pacific climate change
900 in ocean reanalyses and coupled climate models. *JGR Oceans*, **119**, 7066–7077,
901 https://doi.org/10.1002/2014JC009979.

902 Yang, H., J. Liu, G. Lohmann, X. Shi, Y. Hu, and X. Chen, 2016: Ocean-atmosphere
903 dynamics changes associated with prominent ocean surface turbulent heat fluxes
904 trends during 1958–2013. *Ocean Dynamics*, **66**, 353–365,
905 https://doi.org/10.1007/s10236-016-0925-3.

906 Yeager, S. G., and Coauthors, 2023: Reduced Southern Ocean warming enhances global skill
907 and signal-to-noise in an eddy-resolving decadal prediction system. *npj Clim Atmos*
908 *Sci*, **6**, 107, https://doi.org/10.1038/s41612-023-00434-y.

909 Yu, L., 2019: Global Air–Sea Fluxes of Heat, Fresh Water, and Momentum: Energy Budget
910 Closure and Unanswered Questions. *Annu. Rev. Mar. Sci.*, **11**, 227–248,
911 https://doi.org/10.1146/annurev-marine-010816-060704.

912 ——, and R. A. Weller, 2007: Objectively Analyzed Air–Sea Heat Fluxes for the Global Ice-
913 Free Oceans (1981–2005). *Bulletin of the American Meteorological Society*, **88**, 527–
914 540, https://doi.org/10.1175/BAMS-88-4-527.

915 Zaron, E. D., and J. N. Moum, 2009: A New Look at Richardson Number Mixing Schemes
916 for Equatorial Ocean Modeling. *Journal of Physical Oceanography*, **39**, 2652–2664,
917 https://doi.org/10.1175/2009JPO4133.1.

918 Zhuo, J.-Y., C.-Y. Lee, A. Sobel, R. Seager, S. J. Camargo, Y.-H. Lin, B. Fosu, and K. A.
919 Reed, 2025: A More La Niña–Like Response to Radiative Forcing after Flux
920 Adjustment in CESM2. *Journal of Climate*, **38**, 1037–1050,
921 https://doi.org/10.1175/JCLI-D-24-0331.1.

922 Zuo, H., M. A. Balmaseda, and K. Mogensen, 2017: The new eddy-permitting ORAP5 ocean
923 reanalysis: description, evaluation and uncertainties in climate signals. *Clim Dyn*, **49**,
924 791–811, https://doi.org/10.1007/s00382-015-2675-1.

925 ——, M. A. Balmaseda, S. Tietsche, K. Mogensen, and M. Mayer, 2019: The ECMWF
926 operational ensemble reanalysis–analysis system for ocean and sea ice: a description
927 of the system and assessment. *Ocean Sci.*, **15**, 779–808, https://doi.org/10.5194/os-15-
928 779-2019.

929